LOW-PRESSURE PLASMA SYNTHESIS
OF NANOSTRUCTURED COATINGS

O. KYLIÁN

Mathematical and Physical Faculty, Charles University,
V Holešovičkách 2, Prague 8, Czech Republic
E-mail: *ondrej.kylian@gmail.com*

Abstract. Strategy that enables production of nanostructured surfaces is presented. Investigated method is a two-step process based on overcoating of nanoparticles produced by a gas aggregation source by thin film of magnetron sputtered polytetrafluoroethylene. It is shown that surfaces with spatially nonhomogeneous wettability may be produced in this way.

Key words: gas aggregation sources, nanostructured coatings, nanoparticles.

1. INTRODUCTION

Non-equilibrium plasmas are nowadays routinely employed in already impressive range of technological applications, where they are used either for treatment of surfaces or for deposition of various kinds of thin films. Related to latter, numerous strategies that enabled production of smooth thin films of metals, alloys, ceramics, plasma polymers and their nanocomposites with required physico-chemical properties or desired bioadhesive/bio-repellent character were developed in the last few decades. However, recent interest in the production of nanomaterials with unique optical, electrical and biomedical properties triggered off development of novel plasma-based strategies for synthesis of such materials including also so-called gas aggregation sources (GAS) of nanoparticles.

The GAS systems based on magnetron-sputter gas-phase condensation were introduced by Haberland and his co-workers in the 90s of the last century [1]. Unlike other plasma-based techniques, nanoparticles are created in the GAS systems by spontaneous condensation of supersaturated vapor generated by magnetron sputtering in the volume of gas aggregation zone and not on a substrate. Created nanoparticles are then transported by a buffer gas (usually argon) from the aggregation chamber to the main deposition chamber, through an output orifice, in the form of focused beam of nanoparticles. The principal advantage of GAS

systems responsible for their increasing popularity are wide range of materials from which nanoparticles may be produced including metals (*e.g.* [2–6]), metal-oxides (*e.g.* [7, 8]), polymers (*e.g.* [9, 10]) or even hybrid NPs that combine two or more materials (*e.g.* [11–14]). In addition GAS systems may be easily combined with other low pressure plasma-based deposition techniques (*e.g.* PE-CVD, DC, RF or reactive magnetron sputtering). The main aim of this study is to demonstrate that the latter enables fabrication of nanostructured coatings with various architectures. This is going to be shown on combination of Cu NPs and magnetron sputtered tetrafluoroethylene (PTFE) selected as an example that allows highlighting the advantages and perspectives of the use of gas aggregation sources for production of nanostructured and patterned thin films.

2. EXPERIMENTAL

2.1. GAS AGGREGATION SOURCE

Copper nanoparticles (NPs) were produced by simple high vacuum gas aggregation source of own construction that is schematically depicted in Fig. 1. It consisted of a water cooled aggregation chamber with inner diameter 100 mm into which was inserted DC planar magnetron equipped with Cu target (3 mm thick, 3-inch in diameter). The aggregation chamber was ended by a conical lid with an orifice 1.5 mm in diameter. The whole setup was attached onto the main deposition chamber pumped by rotary and diffusion pumps. Argon was used as working gas and its pressure in the aggregation chamber was 40 Pa. Magnetron current was constant in all experiments and equal to 200 mA. The pressure in the main deposition chamber was lower than 0.1 Pa.

The substrates to be coated (one side polished Si wafers (ON Semiconductor) or soda lime glass slides (Marienfeld) were inserted into the deposition chamber by means of a load-lock system. The distance between the output orifice and the substrates was 20 cm and was kept constant in all experiments. Coated area had under these conditions circular shape with diameter of 4 cm. In addition in some experiments either static or movable mask was introduced in between the output orifice of GAS and substrate holder. The mask was in this case 2 mm above the substrate.

Deposition rate of NPs was measured by means of a quartz-crystal microbalance (QCM) positioned below the sample holder. In order to enable acquisition of optical emission spectra of plasma inside the aggregation chamber during NPs production a diagnostic port was positioned in the middle of the aggregation chamber. Optical emission spectra were then recorded by AvaSpec 3648 spectrophotometer (Avantes) in the spectral range 220–900 nm.
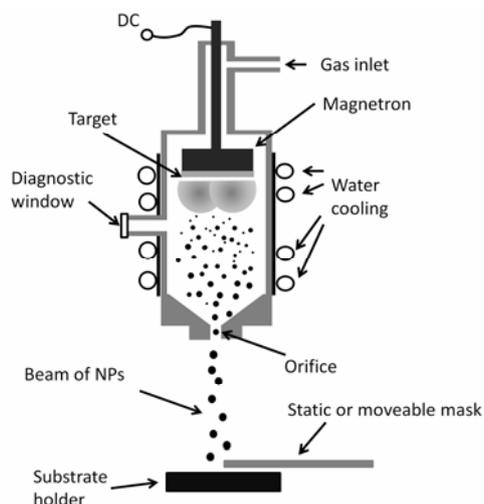
Fig. 1 – Gas aggregation source of Cu nanoparticles.

2.2. MAGNETRON SPUTTERING OF POLYTETRAFLUOROETHYLENE

Fluorocarbon (C:F) films were deposited in a separate deposition chamber equipped with RF, water cooled, planar magnetron with polytetrafluoroethylene (PTFE) target (3mm thick, 81 mm in diameter, Goodfellow). The sputtering was performed in argon atmosphere at pressure of 3 Pa and applied RF power 40 W. Under these conditions the deposition rate was approximately 10 nm/min and the fabricated films were spatially homogeneous with deviations in thickness lower than 10% on 7 cm length of the sample. Details regarding deposition of C:F films may be found elsewhere [15].

2.3. SAMPLES CHARACTERISATION

Optical properties were measured using Hitachi U-2910 spectrophotometer in the spectral range 325–900 nm. The thickness of the fluorocarbon films was evaluated by spectral ellipsometry (Woollam M-2000DI). Wettability of fabricated samples was evaluated by sessile drop method using a goniometer of custom construction. Surface morphology of deposited coatings was determined by means of atomic force microscopy (AFM) and by scanning electron microscopy (SEM). The AFM measurements were done using Quesant Q-Scope 350 that was operated in semi-contact mode using Al coated tips (MULTI75Al-G, Budget Sensors) with tip radius better than 10 nm. SEM analysis was performed using Mira3 (Tescan) scanning electron microscope (accelerating voltage 15 kV).

3. RESULTS AND DISCUSSION

3.1. DEPOSITION OF COPPER NANOPARTICLES

The key step of investigated strategy for production of nanostructured coatings is deposition of copper nanoparticles. As it is depicted in Fig. 2, where an example of SEM image of deposited Cu NPs is presented, produced nanoparticles had approximately spherical shapes. Statistical evaluation of sizes of produced nanoparticles revealed that their sizes ranged from 5 nm up to 50 nm. The mean size was 16 ± 5 nm and the size distribution was log-normal. This is common for NPs produced without any mass filtration and it is sufficient for the most of the application where mono-dispersity is not required.
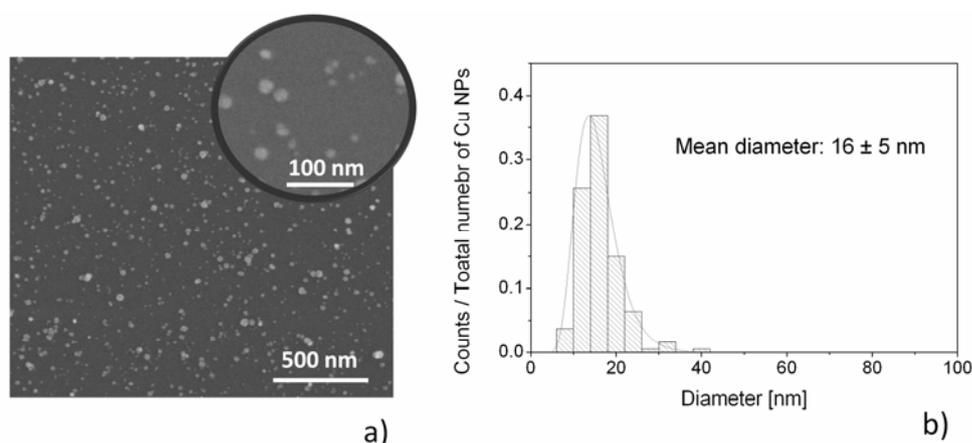

Fig. 2 – SEM image of Cu nanoparticles (left) and corresponding size histogram of produced NPs.

However, the size distribution is not the only parameter crucial for the technological applications. Similarly important are also temporal stability of the deposition process and spatial homogeneity of deposited NPs coatings. In order to check the stability of Cu NPs production magnetron voltage, optical emission spectra of plasma inside the GAS as well as Cu NPs deposition rate were measured. As can be seen in Fig. 3, the intensities of Cu spectral lines, magnetron voltage and deposition rate that is directly proportional to the change of frequency of QCM crystal were temporally stable during the source operation (typically 1 hour of operation).

Concerning the spatial homogeneity of NPs deposition, deposited coatings did not exhibit any visible inhomogeneity. To quantify this qualitative observation, UV-Vis spectra were recorded at different positions on the sample. As can be seen in Fig. 4, acquired UV-Vis spectra exhibited clear absorption peak located at 605 nm that is due to the localized surface plasmon resonance (LSPR) of Cu NPs.

Although the intensity of this peak increases with the deposition time, which reflects the increasing number of deposited Cu NPs, only slight variations of intensity were observed in dependence on the position on the sample (less than 10%). This confirms good spatial homogeneity of deposition process.
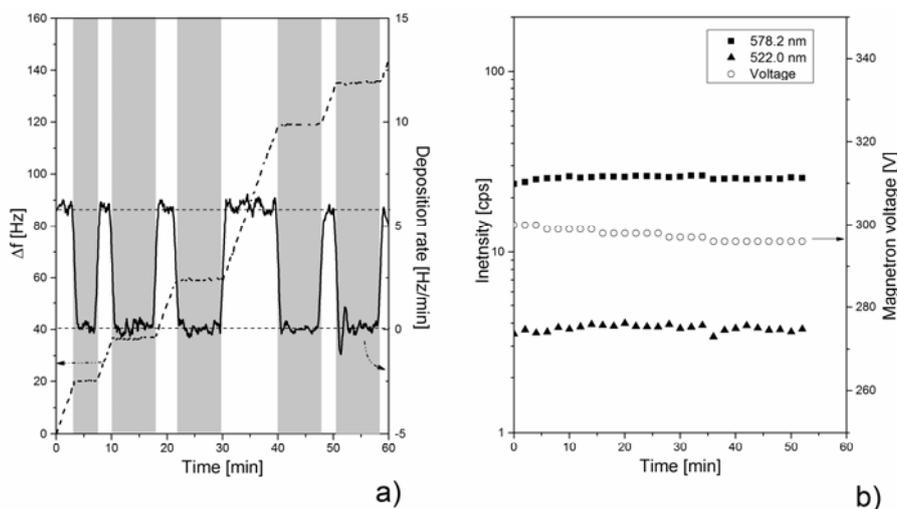

Fig. 3 – a) Deposition rate of Cu NPs measured by quartz crystal microbalance; b) temporal evolutions of magnetron voltage and intensities of Cu spectral lines. The grey zones in a) denote periods when the crystal was shielded from the beam of incoming NPs.
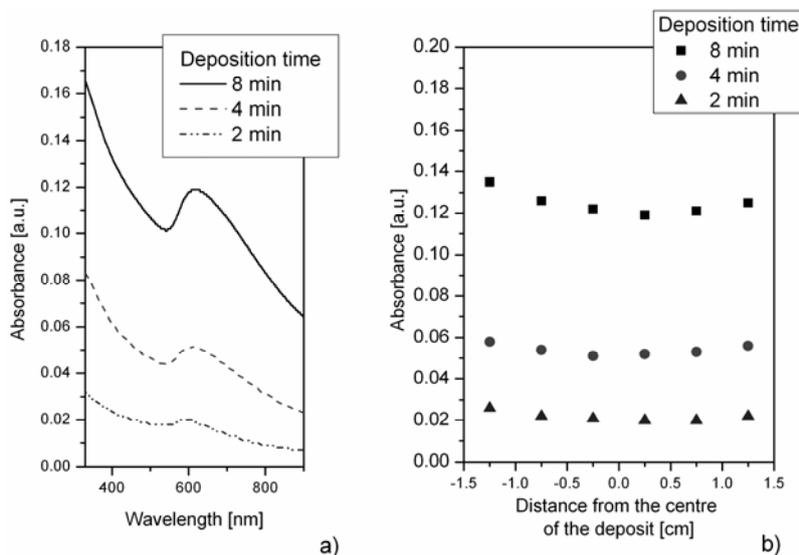

Fig. 4 – a) UV-Vis spectra of films of Cu NPs; b) intensities of Cu absorption peak measured at 605 nm at different positions on the sample.

Another aspect important for the application of gas aggregation source of NPs is the directionality of the deposition process. In order to check this feature that is commonly presumed, a static mask was located above the sample holder that shadowed one side of the sample from the incoming flux of NPs. Visual inspection revealed clear border in between masked area and area exposed to NPs beam. This was further confirmed by AFM analysis of the border area: the sharp border between regions coated and not coated with NPs is distinct also at micrometer scale (width lower than 5µm, Fig. 5a). Experimental confirmation of good directionality of NPs deposition is extremely interesting as it enables to produce different patterns coated with NPs (for examples see Fig. 5b).
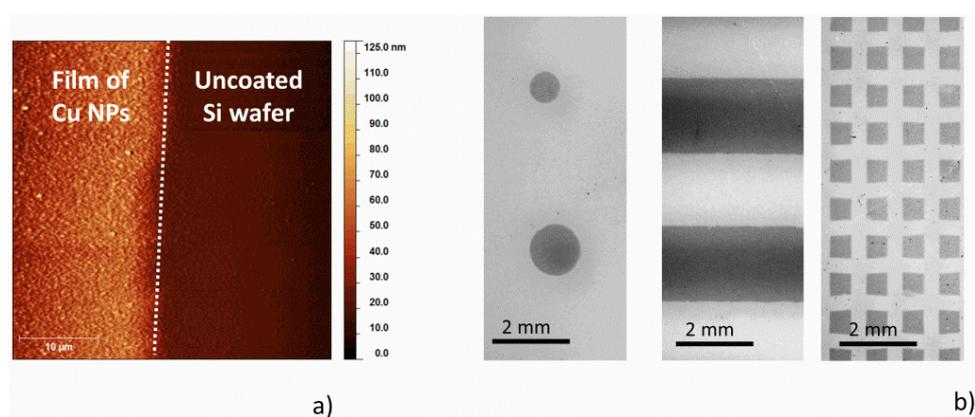

Fig. 5 – a) AFM image of film of Cu NPs deposited through a static mask; b) different patterns fabricated by masks with different geometries. The dark areas correspond to places, where Cu NPs were deposited.

3.2. DEPOSITION OF NANOSTRUCTURED COPPER/C:F COATINGS

Probably the most straightforward way to produce nanostructured films by help of GAS is a two-step process in which the deposited NPs are overcoated by another or the same material. Initially overcoating was performed in order to fix NPs loosely attached to the substrate material and to protect them from the surrounding environment. However, the presence of NPs in the base layer naturally influences also the morphology and with it connected wettability of produced coatings. This was firstly reported for Ti NPs overcoated with either magnetron sputtered Nylon or plasma polymerized nHexane [16]. Similar approach was lately used for other combinations of nanoparticles and overcoat materials [17–19]. Based on these studies it was concluded that the roughness and wettability are strongly dependent on the amount of NPs in the base layer, their size as well as on the thickness of the overcoat layer. In addition, as it will be shown later one, good directionality, stability and homogeneity of beam of incoming NPs demonstrated in

the previous section enables to produce also coatings with nonhomogeneous wettability.

First example of surfaces with spatially variable wetting are surfaces with gradient wettability. Such materials may be produced either by deposition through a mask onto a moving substrate [15] or by deposition onto a static substrate through a moving mask. The second procedure that is easier from the technological point of view was tested in this study. The initial position of the mask was such as to shield the entire substrate from the NP beam (the projection of the edge of the mask in this situation is denoted as position 0 mm on the sample). The mask was subsequently driven in the direction of the sample length at a constant speed (2 cm/min) that made underlaying substrate accessible to incoming Cu NPs. In other words, movement of the mask caused gradual variation of the exposure time of different positions on the substrates to the beam of incoming Cu NPs. Prepared substrates with gradient in amount of deposited Cu NPs were subsequently coated with 20 nm thick film of magnetron sputtered C:F.
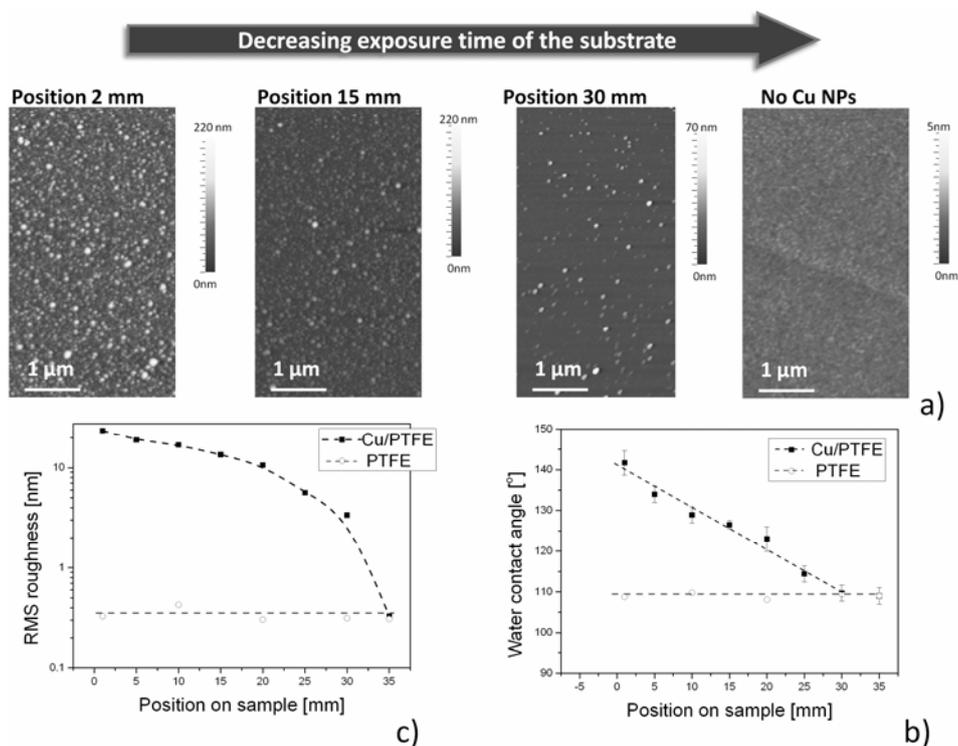

Fig. 6 – a) AFM images of Cu/C:F coatings measured at different positions on gradient sample; b) RMS roughness in dependence on the position on the gradient sample and c) variation of water contact angle with position on the gradient sample. For comparison are presented also values of RMS roughness and water contact angle on smooth C:F film without any Cu NPs.

Due to the different amount of NPs deposited onto different positions on the sample resulting coatings exhibited gradient roughness along the sample length. This is demonstrated in Fig. 6a, where examples of AFM images acquired at different positions on the sample are presented, and in Fig. 6b that shows measured root-mean-square (RMS) roughness in dependence on the position on the sample. As can be seen the RMS roughness gradually increased from 0.3 nm measured on the side, where no Cu NPs were present, up to 24 nm on the side with the highest amount of NPs that formed the base layer. As the smooth film of C:F, *i.e.* film without any Cu NPs, is hydrophobic (static water angle 109°), increase of surface roughness caused increase of water contact angle [20]. For the position on the sample with the highest RMS roughness measured water contact angle reached value 142°.

The different wettability was found to have also impact on the drying of liquid droplets. As it was found droplets of methylene blue/water solution (0,001 mg of methylene blue in 1 ml of H_2O, 3 µl) formed after the water evaporation different patterns on the surface depending on the water contact angle: whereas on the surface sites with water contact angles higher than 126° dried pattern had so-called "coffee ring" shape that is characterized by well-defined, circular and thick outer ring, on sites with lower contact angles were observed irregular patterns, in which the drying material is concentrated into much smaller spots. The transition between the coffee ring formation and irregular spot-like pattern is most likely connected with enhanced pinning of drying droplet on surfaces with more developed nanostructures induced by higher amount of Cu NPs. Possibility to control the coffee ring formation is important finding with respect to possible applications, such as, for instance, Drop coating deposition Raman (DCDR) spectroscopy that is based on analyte preconcentration at the edge of the coffee-ring pattern [21].
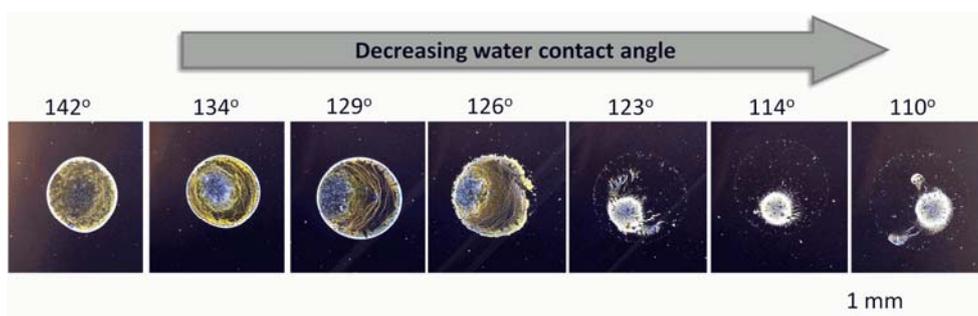

Fig. 7 – White-light micro-images of the dried drops of the methylene blue suspension at different sites on gradient sample. Values of water contact angles are presented for better clarity.

The second example of surfaces with spatially variable wettability represent patterned surfaces with regions with different surface roughness and wettability. In this study a part of substrate surface was shielded from the flux of incoming

Cu NPs by a metallic strip (1 mm thick) and Cu NPs were deposited for 10 min. After overcoating of substrate patterned with Cu NPs with C:F film (20 nm) regions with water contact angle 163° (the regions with Cu NPs in the base layer) and with water contact angle 109° (part of sample without Cu NPs) were easily distinguished. As can be seen in Fig. 8, where are presented top and side views of deposited water droplet, the droplet had shape significantly different from commonly observed rounded one. The droplet was in contact with surface only at the region with higher wettability. In other words the contact between the droplet and surface is confined only to the more wettable strip in between two super-hydrophobic regions. As result of this the water droplet had different apparent water contact angle depending on the direction of observation. Much higher contact angle was observed from the direction parallel to the direction of the hydrophobic strip as compared to the one observed from the direction perpendicular to the direction of the hydrophobic strip. This anisotropy in droplet shape as well as the possibility to fabricate surfaces with well-defined regions with markedly different wettabilities is highly beneficial for production of (bio)sensors or surfaces for fluidic devices.
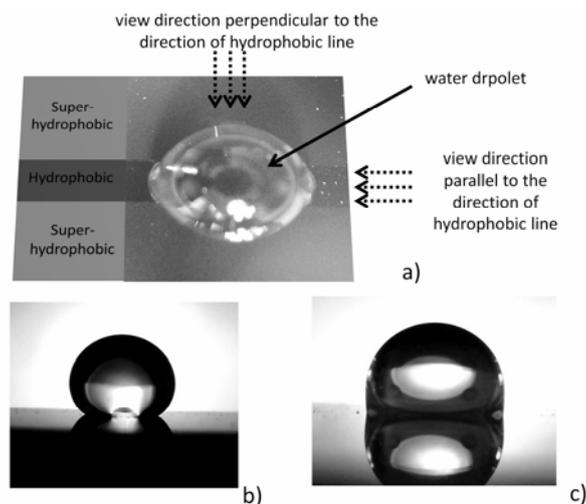

Fig. 8 – a) Top view of water droplet on surface with hydrophobic strip surrounded by super-hydrophobic regions. Side views of water droplet from the direction; b) parallel; c) perpendicular to the direction of hydrophobic strip.

4. CONCLUSION

It was shown that GAS system is highly reliable source of NPs that due to the directionality of deposition process enables to fabricate not only spatially homogeneous NPs coatings, but also patterned or gradient surfaces. This in combination with magnetron sputtering of hydrophobic C:F overlayer deposited on the top of

produced nanoparticle films enabled to synthesize surfaces with tailorable course of wettability. Such materials are highly interesting for various applications that range from fabrication of biosensors to development of fluidic devices.

REFERENCES

1. H. Haberland, M. Karrais, M. Mall and Y. Thurner, J. Vac. Sci. Technol. A **10**, 3266–3271 (1992).
2. S. D'Addato, L. Gragnaniello, S. Valeri, A. Rota, A. di Bona, F. Spizzo, T. Panozaqi and S.F. Schifano, J. Appl. Phys. **107**, 104318 (2010).
3. V. Straňák, S. Block, S. Drache, Z. Hubička, C. A. Helm, L. Jastrabík, M. Tichý and R. Hippler, Surf. Coatings Technol. **205**, 2755–2762 (2011).
4. O. Kylián, V. Valeš, O. Polonskyi, J. Pešička, J. Čechvala, P. Solař, A. Choukourov, D. Slavínská and H. Biederman, Mater. Lett. **79**, 229–231 (2012).
5. T. Acsente, R.F. Negrea, L.C. Nistor, C. Logofatu, E. Matei, R. Birjega, C. Grisolia and G. Dinescu, Eur. Phys. J. D. **69**, 161 (2015).
6. D. Pearmain, S.J. Park, A. Abdela, R.E. Palmer and Z.Y. Li, Nanoscale. **7**, 19647–19652 (2015).
7. A.M. Ahadi, O. Polonskyi, U. Schürmann, T. Strunskus, F. Faupel, J. Phys. D. Appl. Phys. **48**, 35501 (2015).
8. A. Shelemin, O. Kylián, J. Hanuš, A. Choukourov, I. Melnichuk, A. Serov, D. Slavínská and H. Biederman, Vacuum **120**, 162–169 (2015).
9. O. Polonskyi, O. Kylián, P. Solař, a Artemenko, J. Kousal, D. Slavínská, A. Choukourov and H. Biederman, J. Phys. D. Appl. Phys. **45**, 495301 (2012).
10. M. Drábik, A. Serov, O. Kylián, A. Choukourov, A. Artemenko, J. Kousal, O. Polonskyi and H. Biederman, Plasma Process. Polym. **9**, 390–397 (2012).
11. Y.-H. Xu and J.-P. Wang, Adv. Mater. **20**, 994–999 (2008).
12. D. Llamosa, M. Ruano, L. Martínez, A. Mayoral, E. Roman, M. García-Hernández and Y. Huttel, Nanoscale **6**, 3–6 (2014).
13. P. Grammatikopoulos, S. Steinhauer, J. Vernieres, V. Singh and M. Sowwan, Adv. Phys. X. **1**, 81–100 (2016).
14. A. Vahl, J. Strobel, W. Reichstein, O. Polonskyi, T. Strunskus, L. Kienle and F. Faupel, Nanotechnology **28**, 175703 (2017).
15. M. Petr, O. Kylián, J. Hanuš, A. Kuzminova, M. Vaidulych, I. Khalakhan, A. Choukourov, D. Slavínská and H. Biederman, Plasma Process. Polym. **13**, 663–671 (2016).
16. O. Kylián, O. Polonskyi, J. Kratochvíl, A. Artemenko, A. Choukourov, M. Drábik, P. Solař, D. Slavínská and H. Biederman, Plasma Process. Polym. **9**, 180–187 (2012).
17. O. Kylián, M. Petr, A. Serov, P. Solař, O. Polonskyi, J. Hanuš, A. Choukourov and H. Biederman, Vacuum **100**, 57–60 (2014).
18. A. Kuzminova, A. Shelemin, O. Kylián, M. Petr, J. Kratochvíl, P. Solař and H. Biederman, Vacuum **110**, 58–61 (2014).
19. A. Choukourov, O. Kylián, M. Petr, M. Vaidulych, D. Nikitin, J. Hanuš, A. Artemenko, A. Shelemin, I. Gordeev, Z. Kolská, P. Solař, I. Khalakhan, A. Ryabov, J. Májek, D. Slavínska and H. Biederman, Nanoscale **9**, 2616–2625 (2017).
20. R.N. Wenzel, Ind. Eng. Chem. **28**, 988–994 (1936).
21. E. Kočišová and M. Procházka, J. Raman Spectrosc. **42**, 1606-1610 (2011).